KONA Powder and Particle Journal

KONA Powder and Particle Journal No. 43 (2026) 281–294/https://doi.org/10.14356/kona.2026009 Original Research Paper

Machine-Learning-Based Multiscale Methods for 3D Modelling of Granular Materials by Incorporating History-Dependent State Variables †

Mengqi Wang [1], Min Wang [2]*, Shaoheng Guan [1,3] and Yuntian Feng [1]*

[1] *Zienkiewicz Centre for Computational Engineering, Swansea University, UK*
[2] *Fluid Dynamics and Solid Mechanics Group, Theoretical Division, Los Alamos National Laboratory, USA*
[3] *Institute of Theoretical and Computational Physics, Graz University of Technology, Austria*

Over the past decades, the prevalence of machine learning (ML) methods has made the development of ML-based constitutive models for granular materials undoubtedly a popular subject. Numerous studies have been made to feature the loading path or history-dependent stress–strain response of granular media using neural networks. In this work, a novel finite element method (FEM)–ML multiscale approach was developed by incorporating internal variables to improve the simulation accuracy of 3D history-dependent granular materials for the first time. To this end, a surrogate constitutive model based on the single-step-based multi-layer perceptron (MLP) neural network was used to replace representative volume element (RVE) simulations conducted by the discrete element method (DEM) in the multiscale FEM–DEM approach. Although the prediction principle of the MLP aligns with the FEM algorithm, artificially added internal variables are required to differentiate the loading history. To address this issue, history variables associated with the Frobenius norm are proposed to be fed into the MLP coupled with the strain tensor to extract the history-dependent behaviour of granular assemblies. The developed FEM–ML approach was demonstrated in 3D conventional triaxial compression (CTC) simulations. Compared to the multiscale FEM–DEM approach, the proposed FEM–ML method exhibits a significantly improved computational efficiency.

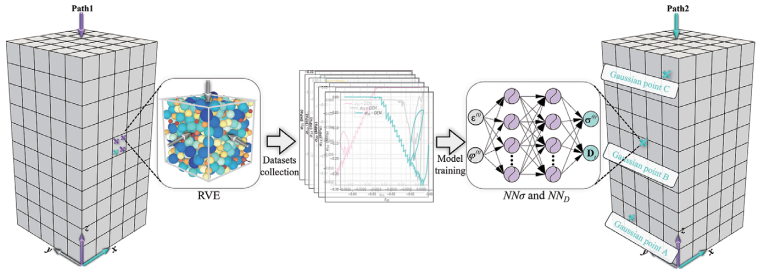

Keywords: path-dependent constitutive response, machine learning, multi-layer perceptron, multiscale modelling, granular materials

1. Introduction

Granular materials consist of discrete particles that interact in ways that are highly dependent on the shape, size, and material properties of the grains. This discrete nature makes the mathematical description of granular systems challenging. At the macroscale, granular materials are typically regarded as a continuous medium and are studied within the framework of continuum mechanics. Recent advancements in continuum phenomenological models have enabled the capture of some complex deformation behaviours of granular media, such as non-coaxiality (Tian and Yao, 2017), strain localisation (Desrues and Andò, 2015), anisotropy (Yin et al., 2010), and path dependence (Hu et al., 2018). However, these continuum-based constitutive models or numerical methods normally smeared out the microscopic features of granular materials at the grain scale (Guo and Zhao, 2014) and thus failed to accurately capture the inherent heterogeneity and discrete nature of granular assemblies. This limitation can lead to an oversimplified representation of critical phenomena like particle interlocking and localised failure mechanisms, which are crucial for understanding the deformation features of granular media under various loading conditions. Additionally, traditional constitutive models tend to be sophisticated for fitting one specific experimental phenomenon, inevitably introducing parameters that lack physical meaning but require significant calibration effort (Qu et al., 2021).

The emergence of the coupled finite element method–discrete element method (FEM–DEM) multiscale approach, bridging the microscale discrete nature to the macrocontinuum feature of granular materials (Andrade and Tu, 2009; Andrade et al., 2011; Guo and Zhao, 2014, 2016; Qu et al., 2021), provides a promising way to solve these challenges. In the FEM–DEM approach, unlike traditional FEM, each Gaussian point in the FE element is assigned an RVE to calculate the local stress response by the DEM and homogenisation (Geers et al., 2010; Li et al., 2010; Miehe et al., 2010) over a particle assembly. This discrepancy allows a more faithful characterisation of the

† Received 27 August 2024; Accepted 1 November 2024
J-STAGE Advance published online 29 April 2025
* Corresponding author: Min Wang; Yuntian Feng;
[1] Add: Swansea, Wales, SA1 8EP, UK
[2] Add: New Mexico 87545, USA
E-mail: minw@lanl.gov (M.W.); y.feng@swansea.ac.uk (Y.F.)
TEL: +1-505667-9155

micro-discrete nature of the granular material and bypasses the phenomenological assumptions. However, the FEM–DEM technique inherently suffers from a significant computational burden because the DEM solver in this approach normally needs to simulate the interaction among a large number of particles, particularly in 3D modelling problems.

Recent machine learning methods enable the development of neural network-based models that can replicate the designated constitutive laws with superior computational efficiency. For instance, Ma et al. (2022) and Qu et al. (2021, 2022) developed a recurrent neural network (RNN)-based constitutive model with the data generated from the discrete element modelling to predict the stress–strain response of granular materials; Wang et al. (2022) explored the feasibility of constructing a temporal convolutional neural network (TCNN)-based model to forecast the constitutive response for granular media. However, all these networks are multi-step-based, which is not compatible well with the single-step-based standard FEM. Despite being integrated into the FEM (Logarzo et al., 2021; Zhang et al., 2021), these time-sequential neural networks face challenges in terms of computational efficiency because their complex architecture introduces too many weighting parameters and results in complex prediction operations.

On the other hand, the single-step-based multi-layer perceptron (MLP) is aligned with the traditional FEM and achieves better computational efficiency; however, it is unable to identify the loading history-dependent mechanical behaviours of granular materials by themselves. Therefore, it requires the assistance of internal/history variables as extra input features (Basheer, 2000, 2002). Earlier this year, Frobenius norms of state variables were proposed by our group (Wang et al., 2024) to improve the MLP-based ML surrogate model for 2D simulations of granular materials. However, a theoretically rigorous and computationally effective method for parameterising history variables for the MLP is still lacking for developing a data-driven multiscale method for real-world 3D granular materials.

The objective of this work is to develop a data-driven multiscale approach for better prediction of the mechanical behaviour of 3D granular materials. To this end, the Frobenius norms of state variables are proposed to assist the MLP in incorporating the history-dependent features of 3D granular materials into the framework of the FEM–ML approach for the first time. The surrogate constitutive model informed by the proposed history variables is trained by an MLP model from many DEM simulations of granular RVE models and validated by predicting the stress response of the RVE with the loading path beyond the training data. Then, the developed FEM–ML computational platform was applied to simulate different triaxial compression tests with different loading paths for validation.

2. History-variable-embedded FEM–ML multiscale method

2.1 The FEM–DEM multiscale framework

As stated in our previous paper (Wang et al., 2024), the FEM–DEM multiscale algorithm comprises two parts: 1) the FEM solver, and 2) the DEM solver. The FEM is responsible for solving the boundary value problem (BVP), and the discrete element modelling provides the constitutive response to each Gaussian integration point. The multiscale FEM–DEM framework was developed by integrating two open-source software packages: 1) Esys-Escript (Gross et al., 2007) provides the function of the FEM solver, and 2) YADE (Smilauer et al., 2023), which provides the DEM solver.

2.1.1 The FEM formulation

In the standard FEM, the deformation of a continuous macroscopic domain Ω is governed by the current nodal displacement $\mathbf{q}_t$ of discretised finite elements and adheres to the equilibrium equation under the quasi-static condition.

$$\int_\Omega \boldsymbol{\sigma}_t \cdot \nabla \mathbf{u}_t \, d\Omega = \int_\Gamma \mathbf{u}_t \cdot \mathbf{t} \, d\Gamma + \int_\Omega \rho \, \mathbf{u}_t \cdot \mathbf{b} \, d\Omega \tag{1}$$

where $\mathbf{u}_t$ is an unknown displacement field function, $\mathbf{u}_t = \mathbf{N} \cdot \mathbf{q}_t$; $\mathbf{N}$ is the shape function; $\mathbf{t}$ and $\mathbf{b}$ represent the traction imposed on Neumann boundary Γ and body force, respectively; ρ is the bulk density of the material; $\boldsymbol{\sigma}_t$ denotes the stress vector of the current load step.

In the FE system, the displacement field $\mathbf{u}_t$ can be solved by minimising the total potential energy $\Pi(\mathbf{q}_t)$ of the Ω according to the principle of minimum potential energy:

$$\prod(\mathbf{q}_t) = \frac{1}{2} \mathbf{q}_t{}^{\mathrm{T}} \mathbf{K}_t \mathbf{q}_t - \mathbf{T} \mathbf{q}_t \tag{2}$$

where $\mathbf{K}_t$ represents the current global stiffness as assembled by the constitutive/tangential operator $\mathbf{D}_t$:

$$\mathbf{K} = \int_\Omega \mathbf{B}^{\mathrm{T}} \mathbf{D}_t \mathbf{B} \, d\Omega \tag{3}$$

$\mathbf{B} = \mathbf{L}\mathbf{N}$ and $\mathbf{L}$ is a differential operator; $\mathbf{T}_t$ represents the external forces of the current load step consisting of the following two items:

$$\mathbf{T}_t = \int_\Gamma \mathbf{N}^{\mathrm{T}} \mathbf{t} \, d\Gamma + \int_\Omega \rho \, \mathbf{N}^{\mathrm{T}} \mathbf{b} \, d\Omega \tag{4}$$

To find the minimum value of the total potential energy of Ω, the partial derivative of $\Pi(\mathbf{q}_t)$ to the nodal displacement $\mathbf{q}_t$ is set to zero:

$$\frac{\partial \prod(\mathbf{q}_t)}{\partial \mathbf{q}_t} = \mathbf{K}_t \mathbf{q}_t - \mathbf{T}_t = 0 \tag{5}$$

In the linear problem, **Eqn. (5)** can be solved directly. While granular materials normally behave highly

nonlinearly, the Newton–Raphson method is leveraged to iteratively solve **Eqn. (5)**:

$$\mathbf{K}_{(t,\,m)}\mathbf{q}_{(t,\,m)} = \mathbf{R}_{(t,\,m)} = \mathbf{T}_t - \mathbf{K}_{(t,\,m\text{-}1)}\mathbf{q}_{(t,\,m\text{-}1)} \tag{6}$$

where $\mathbf{R}_{(t,\,m)}$ is the residual force and the subscript m represents the obtained results of the m-th iteration at the t load step.

2.1.2 RVE-based stress–strain response

In the FEM–DEM multiscale method, the RVE embedded in each Gaussian point provides the local stress response of the granular material. The FEM-solved displacement field $\mathbf{u}$ is sent to the corresponding RVEs in the form of $\nabla\mathbf{u}$, serving as their loading condition. Then, the $\boldsymbol{\sigma}_t$ or $\mathbf{D}_t$ are derived from each RVE by the DEM and are returned to the FEM solver to drive the macroscopic simulation for the next round iteration.

In the DEM, the interparticle contact relationships govern the stress tensor and tangential operator of a particle assembly. With different homogenisation hypotheses, such as Voigt's hypothesis (Kruyt and Rothenburg, 1998), the stress tensor can be obtained as follows:

$$\sigma = \frac{1}{\mathrm{V}}\sum_{\mathrm{Nc}} \mathbf{d}^{\mathrm{c}} \otimes \mathbf{f}^{\mathrm{c}} \tag{7}$$

where N_c is the total number of contact pairs.

The tangential operator can be estimated from the homogenised modulus of the packing as follows (Guo and Zhao, 2016):

$$\mathbf{D} = \frac{1}{\mathrm{V}}\sum_{\mathrm{Nc}} (k_{\mathrm{n}}\mathbf{n}^{\mathrm{c}} \otimes \mathbf{d}^{\mathrm{c}} \otimes \mathbf{n}^{\mathrm{c}} \otimes \mathbf{d}^{\mathrm{c}} + k_{\mathrm{t}}\mathbf{t}^{\mathrm{c}} \otimes \mathbf{d}^{\mathrm{c}} \otimes \mathbf{t}^{\mathrm{c}} \otimes \mathbf{d}^{\mathrm{c}}) \tag{8}$$

where $\mathbf{n}^{\mathrm{c}}$ and $\mathbf{t}^{\mathrm{c}}$ are the contact norm and tangential vectors, respectively; $\mathbf{d}^{\mathrm{c}}$ is the branch vector connecting the centres of two particles and $\mathbf{t}^{\mathrm{c}}$ denotes the contact force between them.

To compute $\mathbf{f}^{\mathrm{c}} = \mathbf{f}_{\mathrm{n}}^{\mathrm{c}} + \mathbf{f}_{\mathrm{t}}^{\mathrm{c}}$ at one contact, Hertz's contact model is employed in this work. The normal contact force $\mathbf{f}_{\mathrm{n}}^{\mathrm{c}}$ is given by $\mathbf{f}_{\mathrm{n}}^{\mathrm{c}} = -k_{\mathrm{n}}\delta\mathbf{n}^{\mathrm{c}}$ and the tangential contact force $\mathbf{f}_{\mathrm{t}}^{\mathrm{c}}$ is calculated as $\mathbf{f}_{\mathrm{t}}^{\mathrm{c}} = -k_{\mathrm{t}}\delta\mathbf{u}^{\mathrm{t}}$ and $\| \mathbf{f}_{\mathrm{t}}^{\mathrm{c}} \| \leq \mu \| \mathbf{f}_{\mathrm{n}}^{\mathrm{c}} \|$, where k_{n} and k_{t} represent the norm and tangential contact stiffness, respectively; δ represents the overlap between two contacted grains; $\mathbf{u}^{\mathrm{t}}$ is the tangential displacement; μ is the friction coefficient.

2.2 The history variables-embedded ML constitutive model

The remarkable mapping capability and high computational efficiency of the data-driven method make it a promising approach for describing the stress–strain response of granular media. However, the constitutive behaviour of a particle collection is normally history-dependent, and solving this time-sequence problem is a key challenge that influences the construction of ML surrogate constitutive models.

2.2.1 History-dependent behaviour of ML constitutive models

Both single-step and time-sequence neural networks are extensively leveraged to model the history-dependent constitutive response of granular materials. With specific architectures, time-sequence networks, such as the gated recurrent unit (GRU) and long short-term memory (LSTM), naturally consider historical strain states to predict the stress state $\hat{\boldsymbol{\sigma}}^{(t)}$ of the current time step. However, their multi-step nature is contrasted with the single-step-based FEM, and the complex network structure makes them not sufficiently efficient to be trained. Thus, they are less ideal for developing FEM–ML schemes.

On the other hand, as shown in **Fig. 1**, although single-step-based networks like MLP are aligned to the standard FEM algorithm, their predicted stress $\hat{\boldsymbol{\sigma}}^{(t)}$ depends solely on the current strain state $\boldsymbol{\varepsilon}^{(t)}$ by:

$$\hat{\boldsymbol{\sigma}}^{(t)} = f^{\mathrm{MLP}}(\boldsymbol{\varepsilon}^{(t)}, \mathbf{W}\{\mathbf{W_1}, \mathbf{W_2}, \mathbf{W_3}\}, \mathbf{b}\{\mathrm{b}_1, \mathrm{b}_2, \mathrm{b}_3\}) \tag{9}$$

where $\mathbf{W}$ and $\mathbf{b}$ represent trainable parameters; thus, no history information is explicitly considered. Therefore, the artificially added internal/history variables φ must feature the loading history, i.e., unloading and reloading.

There are typically two methods to select the history variables for single-step-based networks, as illustrated in **Fig. 2**. The first scheme leverages the predicted state arguments as history variables. For example, as shown in **Fig. 2(a)**, literatures (Basheer, 2002; Drakos and Pande, 2015; Hashash and Song, 2008; Sidarta and Ghaboussi, 1998) employ the predicted stress state $\hat{\boldsymbol{\sigma}}^{(t-1)}$ and the strain state $\boldsymbol{\varepsilon}^{(t-1)}$ at last time step as history variables. The second approach (Huang et al., 2020; Wang et al., 2024) directly features history variables from the current state parameters

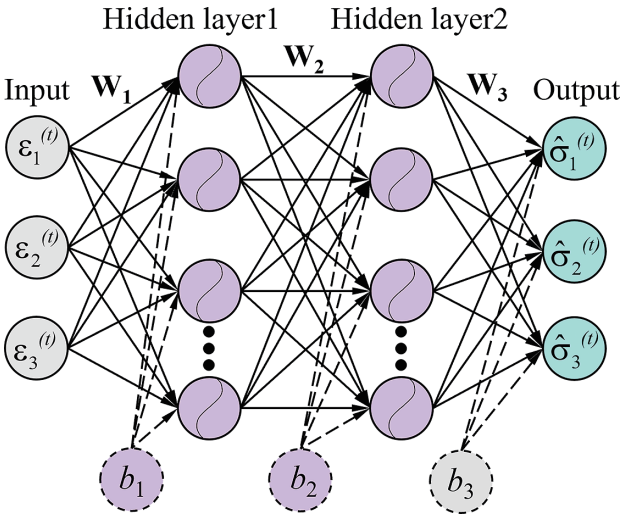

Fig. 1 Basic architecture of MLP.

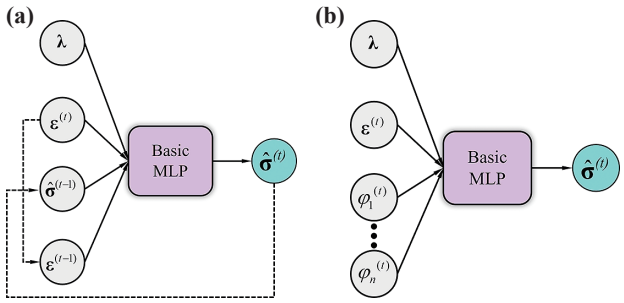

Fig. 2 Different methods for selecting history variables for MLP: **(a)** Scheme 1; **(b)** Scheme 2.

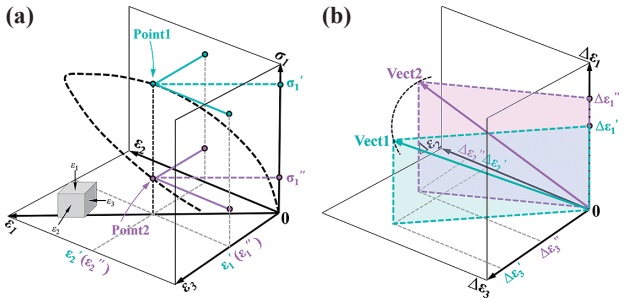

Fig. 3 Principles for selecting history variables: **(a)** the stress–strain relation under reversal CTC loading case; **(b)** the different loading paths to one stress–strain state.

(see **Fig. 2(b)**) where λ represents the material parameters of the granular media. Compared to the second method, an unavoidable issue in the first scheme is that any prediction errors in the state variables affect the next time-step prediction, which introduces the accumulated errors to the network and can ultimately lead to the breakdown of the entire prediction system. In addition, the prediction process in the first scheme runs serially, which is less efficient than the second approach, where the prediction for each time step is independent. Despite these advantages of the second approach, the parameterisation of history variables remains a tricky issue.

2.2.2 Parameterisation of internal variables based on state variables

In this work, to replace the function of RVE in the FEM–DEM method using the ML method, an MLP-based constitutive model, which can capture the loading history, was developed. As shown in **Fig. 3(a)**, in one CTC loading case, which includes the unloading and reloading stages, the situation where the same strain state (e.g. the strain state at both Point1 and Point2) corresponding to different stress states (i.e. $\boldsymbol{\sigma}_1'$ and $\boldsymbol{\sigma}_1''$) occurs. Consequently, internal variables are required as the extra inputs of the MLP to transfer the "one-to-many" mapping to a surjective ("one-to-one" or "many-to-one") such that the MLP can learn the loading history-dependent stress–strain relationship, which can be formulated as follows:

$$\hat{\boldsymbol{\sigma}}^{(t)} = f^{\mathrm{MLP}}(\boldsymbol{\varepsilon}^{(t)}, \boldsymbol{\varphi}^{(t)}\{\varphi_1{}^{(t)}, \ldots, \varphi_n{}^{(t)}\}, \mathbf{W}, \mathbf{b}) \tag{10}$$

where $\boldsymbol{\varphi}^{(t)}$ represents history-dependent state variables.

To avoid the error accumulation problem discussed in **Section 2.2.1**, this work selects state variables of the current time step. However, unlike phenomenological models, the DEM performs history-dependent constitutive behaviour by updating the kinematic characteristics and contact forces between particles by physically intuitive contact laws along the timeline, leading to the absence of explicit internal variables available to represent the loading history for MLP models. Consequently, it is crucial to visualise history parameters from the state variables of the RVE to assist the ML model in learning the different loading states of the granular media.

In this study, a novel parameterisation scheme for history variables is proposed based on the following principles: 1) the history variables used in MLP should not introduce accumulated errors to the prediction system; 2) the history variables can be directly extracted from the RVE model without extra experiment; 3) the loading history should be characterised with the minimum number of internal variables in the MLP to reduce the computational burden in both the data generation and network training processes.

In FEM–DEM modelling, the accumulated absolute strain increment $\Delta\varepsilon_{ij}^{(t)}$ of each RVE is one of the easiest measurable physical variables. It indicates the accumulated deformation of the material in a specific direction at the current time step and can be obtained from the strain sequence as follows:

$$\Delta\varepsilon_{ij}{}^{(t)} = \begin{cases} 0, & t = 0 \\ \sum_{k=1}^{t} \left|\varepsilon_{ij}{}^{(t)} - \varepsilon_{ij}{}^{(t\text{-}1)}\right|, & t \geq 1 \end{cases} \tag{11}$$

where the subscripts $i, j \in \{1, 2, 3\}$ in the 3D problem, and a total of six independent components are included in this tensor, which is coordinate-dependent. Inspired by the Frobenius norm (F-norm), which integrates the effects of all elements of a tensor, the $\Delta\varepsilon_{ij}^{(t)}$ is further condensed into a single variable $\|\Delta\boldsymbol{\varepsilon}^{(t)}\|_{\mathrm{F}}$:

$$\varphi_1{}^{(t)} = \left\|\Delta\boldsymbol{\varepsilon}^{(t)}\right\|_{\mathrm{F}} := \sqrt{\sum_{i=1}^{3}\sum_{j=1}^{3}\left|\Delta\varepsilon_{ij}{}^{(t)}\right|^2} \tag{12}$$

This variable, which provides a non-negative scalar value for integrating the deformation history, is adopted as the first primary history variable $\varphi_1{}^{(t)}$ in this study. Its non-negative and monotonically increasing nature ensures a mathematical surjective between the input and output features of the MLP, effectively encoding the loading history.

In addition, it is important to account for the uniqueness of the strain path when characterising the history variables of the MLP. As illustrated in **Fig. 3 (b)**, different strain

paths can correspond to the same $\|\Delta\varepsilon^{(t)}\|_F$, such as the ***Vect*1** ($\Delta\varepsilon_1'$, $\Delta\varepsilon_2'$, $\Delta\varepsilon_3'$) and ***Vect*2** ($\Delta\varepsilon_1''$, $\Delta\varepsilon_2''$, $\Delta\varepsilon_3''$). Consequently, unlike our 2D work (Wang et al., 2024), in which at least two internal variables are required to aid the MLP in capturing the different loading history, the 3D problem necessitates the use of at least three internal variables to ensure that the single-step-based neural network model learns the unique strain path of the current load step.

In this study, the trace of the accumulated absolute strain increment, $\Delta\varepsilon_{ij}^{(t)}$, representing the accumulated volumetric changes, is employed as the second history variable $\varphi_2^{(t)}$. This variable enables the MLP model to differentiate between various deformation modes, particularly those involving dilatational effects that cannot be fully captured by $\varphi_1^{(t)}$. Additionally, a non-negative scalar, computed as the product of all $\Delta\varepsilon_{ij}^{(t)}$ components, is introduced as the third history variable $\varphi_3^{(t)}$, to ensure the uniqueness of the loading path in combination with $\varphi_1^{(t)}$ and $\varphi_2^{(t)}$. The second and third history variables are, respectively, formulated as follows:

$$\varphi_2^{(t)} = \Delta\varepsilon_{ij}^{(t)} \tag{13}$$

$$\varphi_3^{(t)} = \prod_{i=1}^{3}\prod_{j=1}^{3}\Delta\varepsilon_{ij}^{(t)} \tag{14}$$

Therefore, by replacing the RVE embedded in each Gaussian point, the ML surrogate model used in this study can be expressed as follows:

$$\hat{\boldsymbol{\sigma}}^{(t)} = f^{\mathrm{MLP}}(\boldsymbol{\varepsilon}^{(t)}, \boldsymbol{\varphi}^{(t)}\{\varphi_1^{(t)}, \varphi_2^{(t)}, \varphi_3^{(t)}\}, \mathbf{W}, \mathbf{b}) \tag{15}$$

This work validates the feasibility and reliability of the proposed parameterising scheme for history variables through a specific ML-based finite element modelling.

2.3 RVE data-based FEM–ML approach

The core idea behind constructing the data-driven multiscale computational platform involves substituting the function of the DEM solver in the FEM–DEM approach with the ML models. **Section 2.2.2** describes how to replace the RVE with an MLP to describe the constitutive laws of granular media in the 3D stress–strain space. This section further discusses how to use the ML method to provide the tangential operator of granular materials, which governs the update direction of the Newton–Raphson iteration in implicit FEM, and finally to build the history-information-embedded FEM–ML framework. In some studies focusing on the development of a data-driven FEM–ML framework (Ghavamian and Simone, 2019; Hashash et al., 2004), the automatic differentiation (AD) method was used to directly approximate the tangential operator ($\mathbf{D} = \partial\boldsymbol{\sigma}/\partial\boldsymbol{\varepsilon}$) or global stiffness matrix by $\mathbf{K} = \partial\mathbf{f}/\partial\mathbf{u}$. This approach is feasible because the constitutive models adopted at each Gaussian point are sufficiently smooth. However, the stress–strain response of an RVE, which is a collection of particles, exhibits significant fluctuations, making the AD approach not suitable for this study.

Alternatively, in the proposed FEM–ML approach, another trained MLP provides the prediction of the tangential operator. This is theoretically feasible because the strain state and tangent stiffness matrix **D** can also maintain a rigorous "one-to-one" mapping with the assistance of the added history variables.

However, unlike the work on 2D problems (Wang et al., 2024), where the MLP model can directly predict all 16 components of the tangential operator with relative ease due to the simpler strain and stress relationships, accurate prediction for the 81 components of **the D** matrix becomes significantly challenging in 3D problems.

To solve this challenge, considering that there are six independent components in the strain and stress tensor and the symmetry of **D**, only the following 21 components marked in **Eqn. (16)** are predicted to strike a balance between accuracy and computational efficiency while still accounting for the necessary history variables to ensure a unique and robust mapping.

$$\mathbf{D} = \begin{pmatrix} D_{1111} & D_{1112} & D_{1113} & D_{1122} & D_{1123} & D_{1133} \\ & D_{1212} & D_{1213} & D_{1222} & D_{1223} & D_{1233} \\ & & D_{1313} & D_{1322} & D_{1323} & D_{1333} \\ & & & D_{2222} & D_{2223} & D_{2233} \\ & & & & D_{2323} & D_{2333} \\ & & & & & D_{3333} \end{pmatrix} \tag{16}$$

Then, the matrix **D** is reassembled and restored to 81 components to construct the global stiffness of the FE solution. Therefore, as shown in **Fig. 4**, two MLP models can be trained in the proposed FEM–ML scheme to provide the stress and tangent stiffness matrix for each Gaussian point, respectively, which can be formulated as follows:

$$\begin{cases} \boldsymbol{\sigma}^{(t)} = f^{\mathrm{NN}_\sigma}(\boldsymbol{\varepsilon}^{(t)}, \{\varphi_1^{(t)}, \varphi_2^{(t)}, \varphi_3^{(t)}\}, \mathbf{W}, \mathbf{b}) \\ \mathbf{D}_t = f^{\mathrm{NN}_D}(\boldsymbol{\varepsilon}^{(t)}, \{\varphi_1^{(t)}, \varphi_2^{(t)}, \varphi_3^{(t)}\}, \mathbf{W}, \mathbf{b}) \end{cases} \tag{17}$$

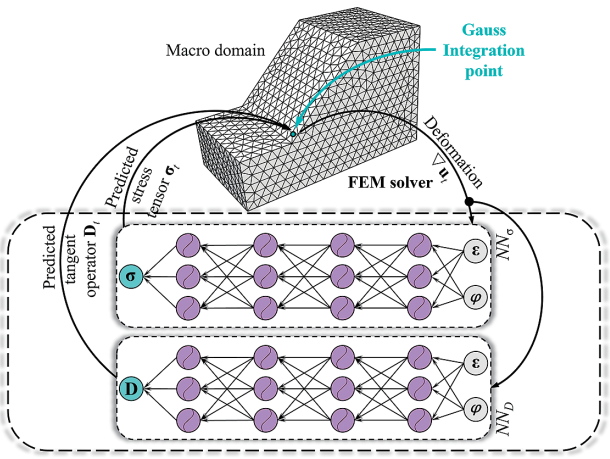

Fig. 4 The proposed FEM–ML approach for solving 3D problems.

The detailed network structures and training parameters of these two neural networks, including the number of hidden layers, nodes in each layer, and learning rate, are listed in **Table 3** in **Section 3.2**. The neural networks used in this study are implemented using the PyTorch library.

3. Validation of the MLP surrogate models

In this section, two triaxial compression simulations are performed using FEM–DEM multiscale method on the same 5 × 5 × 10-FE mesh but under two different loading paths. Partial modelling data generated under the first loading path are used to train two MLPs that provide the constitutive response and tangential operator of the Gaussian points for the FEM solver. The modelling conducted under the second loading path was regarded as a contrast experiment.

3.1 Data generation by FEM–DEM modelling

3.1.1 Preparation of the RVE for each Gaussian point

In the FEM–DEM multiscale simulation, the stress–strain response of the RVE embedded in each Gaussian point intrinsically controls the macroscopic deformation of the granular media. Therefore, preparing an RVE is crucial for hierarchical multiscale modelling. For a specific problem, the parameters of the particle, such as roundness, roughness, and sphericity, in the RVE should be carefully calibrated. However, the primary purpose of the current work was to validate the methodology of constructing the FEM–ML framework; thus, the simplest spherical particle was used for demonstration.

The stress response of an RVE composed of a few particles exhibits significant deviations under the same loading condition. Although the increased number of particles in the RVE can relieve this problem, excessive grains in each RVE can result in a computational burden in the FEM–DEM simulation. To accelerate solving the local stress state by the RVEs while ensuring their stable performance, 1000 particles are encompassed into each RVE, which has been demonstrated as an ideal choice in FEM–DEM multiscale simulation in the literature (Guo and Zhao, 2016; Thornton, 2000; Wang and Zhang, 2021). The detailed particle parameters used in the RVE are listed in **Table 1**.

Furthermore, before conducting the triaxial compression modelling, each RVE was isotropically consolidated to 100 kPa along three principal directions with a friction coefficient of zero, which was restored to 0.5 during the FEM–DEM multiscale modelling.

3.1.2 The triaxial compression modelling with the FEM–DEM method

In this section, as shown in **Figs. 5(a)** and **(c)**, respectively, two triaxial compression FEM–DEM models are conducted using the same cuboid specimen, each with a height of 1.0 m and a square cross-section with a side length of 0.5 m. In each multiscale simulation, first-order accuracy was adopted during the FEM solving process, meaning that only eight Gaussian points are utilised in each cubic finite element, as shown in **Fig. 5(b)**. As discussed in **Section 3.1.1**, the pre-isotropically consolidated RVE comprising 1000 particles was prepared and embedded in Gaussian points of the FE element, providing the local constitutive response for the specimen. Eventually, (5 × 5 × 10 × 8) 2000 RVEs are used in each FEM–DEM simulation.

Based on the meshed specimen, these two triaxial compression models were respectively conducted under the same boundary condition but with different reversal loading paths (i.e., *Path1* and *Path2*), as shown in **Fig. 6**. In each simulation, the bottom of the sample was fixed and displacement-controlled axial loading was applied to the top surface of the specimen until the axial strains arrived at 4.5 % along different loading paths. Furthermore, a confining stress of 100 kPa was applied to the vertical and lateral faces of the specimen during the initial loading stage.

The stress–strain curves of 1500 randomly selected Gaussian points under the loading *Path1* were employed to develop the MLP model. Based on our previous experience (Qu et al., 2023; Wang et al., 2022; Wang et al., 2024), 1500 samples were sufficient for training. We validate it later in this section. The simulation result obtained under loading path 2 serves as a validation test and is compared

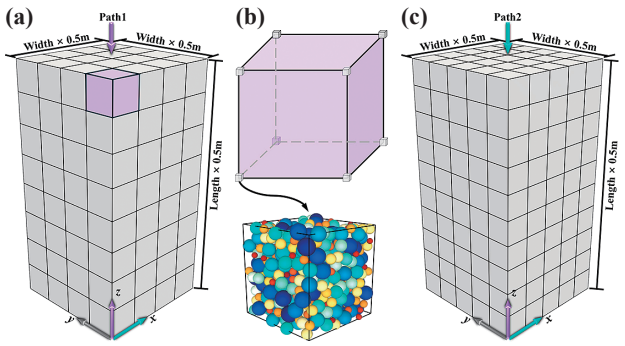

Fig. 5 Setup for the FEM–DEM modelling for triaxial compression: **(a)** Modelling under *Path1*; **(b)** Cubic finite element; **(c)** Modelling under *Path2*.

Table 1 Particle parameters for each RVE used in FEM–DEM modelling.

Particle number	Particle size range (m)	Mean particle diameter (m)	Density (kg/m^3)	Frictional coefficient μ	Elastic modulus E (GPa)	Poisson's ratio v
1000	0.002–0.008	0.005	2650	0.5	0.3	0.3

with the result obtained by the constructed FEM–ML scheme under the same boundary conditions and meshes. The detailed parameters used in these two simulations are listed in **Table 2**.

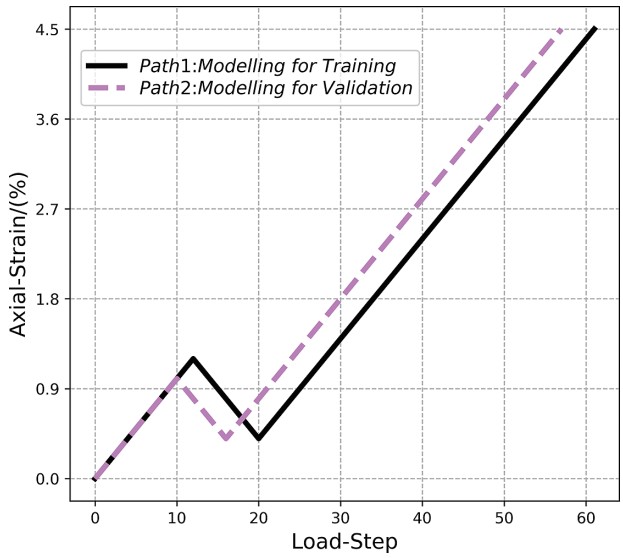

Fig. 6 Different reversal loading paths in the two FEM–DEM simulations.

3.2 MLPs training in the FEM–ML framework

As discussed in **Section 2.3**, the FEM–ML method requires two MLP models: NN_σ to predict the local stress of granular materials for validation and NN_D to provide the tangent stiffness matrix for the FEM solver. The strain, stress tensor, and tangential operator of randomly selected 1500 Gaussian points generated during Simulation 1 in **Table 2** were collected to train these two neural network models, NN_σ and NN_D. The datasets of the remaining 500 Gaussian points were excluded during the training stage. For illustration, parts of stress–strain paths of the training set are given in **Fig. 7**.

Before training these two MLP models, each variable in the training set was normalised to the range of (0, 1) by

$$X_{norm} = \frac{x - X_{min}}{X_{max} - X_{min}} \tag{18}$$

where X_{min}, X_{max}, and X_{norm} denote the minimum, maximum and normalised values of each variable. Then, these normalised input features comprising six independent strain components $\{\varepsilon_{11}^{(t)}, \varepsilon_{12}^{(t)}, \varepsilon_{13}^{(t)}, \varepsilon_{22}^{(t)}, \varepsilon_{23}^{(t)}, \varepsilon_{33}^{(t)}\}$ and three proposed history variables $\{\varphi_1^{(t)}, \varphi_2^{(t)}, \varphi_3^{(t)}\}$ are fed into two different MLPs to respectively predict the

Table 2 Detailed parameters used in two FEM–DEM multiscale models.

No.	Method	Loading path	Data for using	Total load steps	Time (h)	Unloading step	Reloading step	Number of RVEs
1	FEM–DEM	*Path1*	Training	61	29.7	11	20	2000
2	FEM–DEM	*Path2*	Validation	57	24.8	10	16	2000

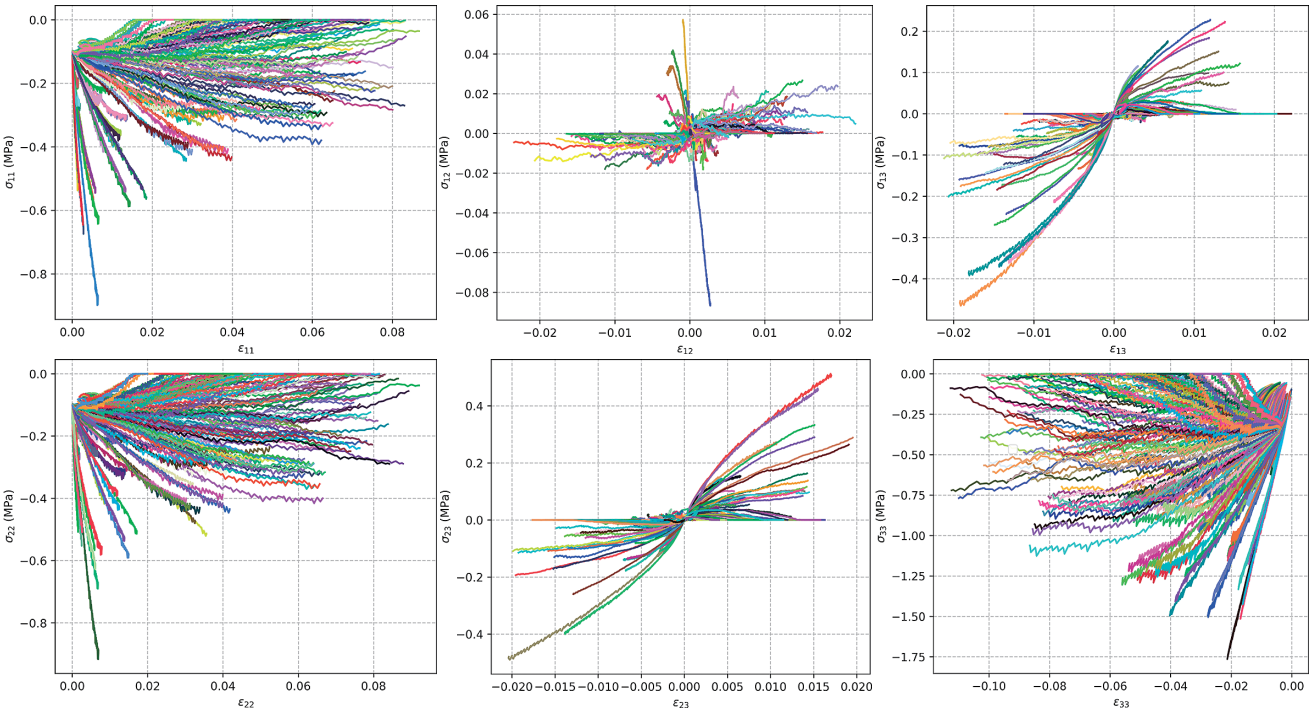

Fig. 7 The partial stress–strain paths of the training data.

corresponding six stress components and the 21 elements of the tangential matrix. The detailed training parameters of each MLP model are listed in **Table 3**.

During the training process, the mean absolute error (MAE) was adopted as the metric to quantify the error between the predicted value of the MLP and the ground truth. The training results of the NNσ and NN_D are presented in **Fig. 8**.

3.3 Validation of the proposed surrogate models

In this section, two well-trained MLPs (**Section 3.2**) are embedded into the Gaussian points of the meshed specimen to solve the identical BVP with the Simulation 2 in **Table 2** under the loading *Path2*. During the FEM–ML modelling process, both the information of each Gaussian point (i.e. stress–strain response and tangential operator) and the solved macroscopic simulation results were recorded. The results obtained by the developed FEM–ML strategy are then compared with those obtained from Simulation 2 in **Table 2**, aiming to provide a comprehensive assessment of the developed data-driven multiscale framework.

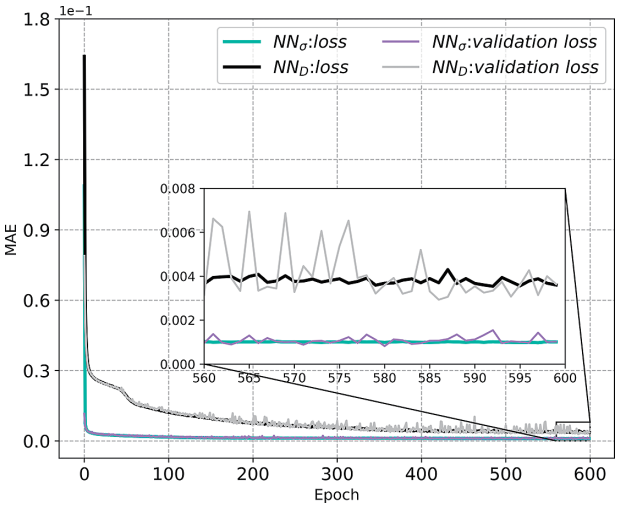

Fig. 8 Training results of NN_σ and NN_D.

3.3.1 The prediction of stress–strain response of Gaussian points by MLP

As displayed in **Fig. 9**, the loading data collected from selected 1500 Gaussian points (marked in purple colour) from Simulation 1 in **Table 2** are used to train NN_σ and NN_D with the assistance of the proposed history variables. Gaussian points whose data were not exposed during the training stage are indicated in green. The trained models were then encapsulated into each Gaussian point of the FE mesh to solve the same BVP but under the loading *Path2*. The stress solutions of all the Gaussian points obtained by these two MLPs during the FEM–ML simulation were compared with those obtained from corresponding FEM–DEM modelling in **Table 2**.

Fig. 10 shows the error between the stress states of the Gaussian points solved by the DEM solver and the MLP. The colour within each marker represents the absolute prediction error. These prediction results demonstrate that the performance of the MLP-based constitutive model is comparable to that of the DEM solver in terms of stress

Table 3 The training parameters used in NN_σ and NN_D models.

Network	Hidden layers	Units in each layer	Batch size	Learning rate	Epoch	Input features	Output features
NNσ	4	20	64	0.0001	600	$\{\varepsilon_{11}^{(t)}, \varepsilon_{12}^{(t)}, \varepsilon_{13}^{(t)}, \varepsilon_{22}^{(t)}, \varepsilon_{23}^{(t)}, \varepsilon_{33}^{(t)}, \varphi_1^{(t)}, \varphi_2^{(t)}, \varphi_3^{(t)}\}$	$\{\sigma_{11}^{(t)}, \sigma_{12}^{(t)}, \sigma_{13}^{(t)}, \sigma_{22}^{(t)}, \sigma_{23}^{(t)}, \sigma_{33}^{(t)}\}$
NN_D	4	20	64	0.0001	600	$\{\varepsilon_{11}^{(t)}, \varepsilon_{12}^{(t)}, \varepsilon_{13}^{(t)}, \varepsilon_{22}^{(t)}, \varepsilon_{23}^{(t)}, \varepsilon_{33}^{(t)}, \varphi_1^{(t)}, \varphi_2^{(t)}, \varphi_3^{(t)}\}$	$\{\mathbf{D}_{(t)}\}$

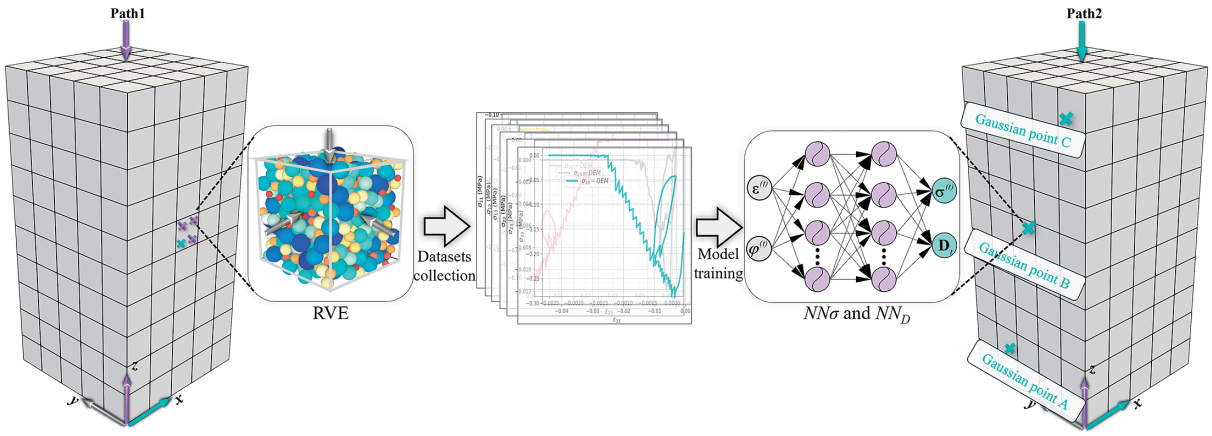

Fig. 9 Validation scheme of trained MLPs.

calculation.

In addition to the overall predictions of the stress and tangential operator at all Gaussian points, as shown in **Fig. 9**, the predicted stress–strain responses of three specific Gaussian points whose loading data are not included in the training stage are also plotted in **Figs. 11**, **12**, and **13**, respectively. The results demonstrate that the trained NN_{σ} can effectively differentiate different loading histories and capture the complex constitutive laws of granular materials using the proposed history variables.

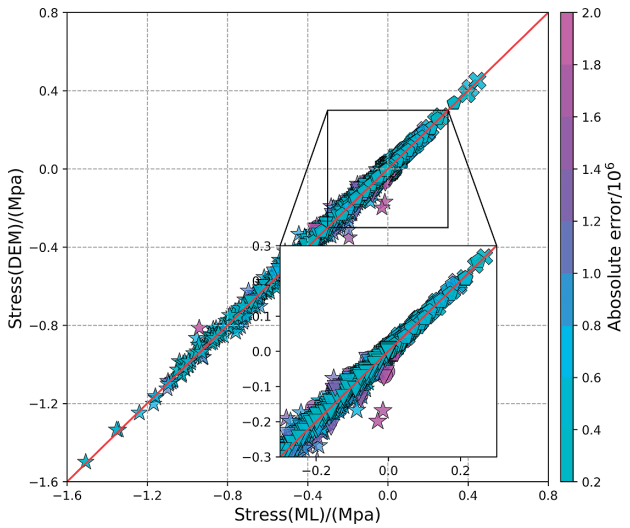

Fig. 10 Absolute errors between the predicted stress and ground truth for all Gaussian points under the loading *Path2*.

3.3.2 FEM–ML for the triaxial compression modelling

In addition to validating the developed FEM–ML approach on the RVE scale, it is important to assess its performance in solving the BVP across the whole specimen. In this section, the axial displacement field, shear strain, and stress distribution obtained by the FEM–ML method are compared with those obtained from Simulation 2 FEM–DEM modelling in **Table 2**. A detailed comparison of the FEM–DEM and FEM–ML triaxial compression models is presented in **Table 4**.

Fig. 14 presents the axial displacement fields obtained by both FEM–DEM and FEM–ML methods under the loading *Path2*, along with the changes in the force at the top surface. **Fig. 14(a)**, **(b)**, and **(c)** respectively plot the axial displacement distributions of the computational domain at the 4th, 16th and 57th load steps. These special moments are highlighted in **Fig. 14(d)** where the axial deformation remains constant at the 4th and 16th load steps and reaches its maximum at the 57th load step.

Similarly, the shear strain distributions in the computational domain at the 4th, 16th and 57th loading steps are showcased in **Fig. 15(a)**, **(b)**, and **(c)**, respectively. It is found that the maximum shear strain at the 16th loading step is larger than that at the 4th loading step. This occurred because the sample had entered the plastic state before the unloading process, resulting in additional plastic deformation. Additionally, the changes in the volume strain of the specimen under loading *Path2* are demonstrated in **Fig. 15(d)**.

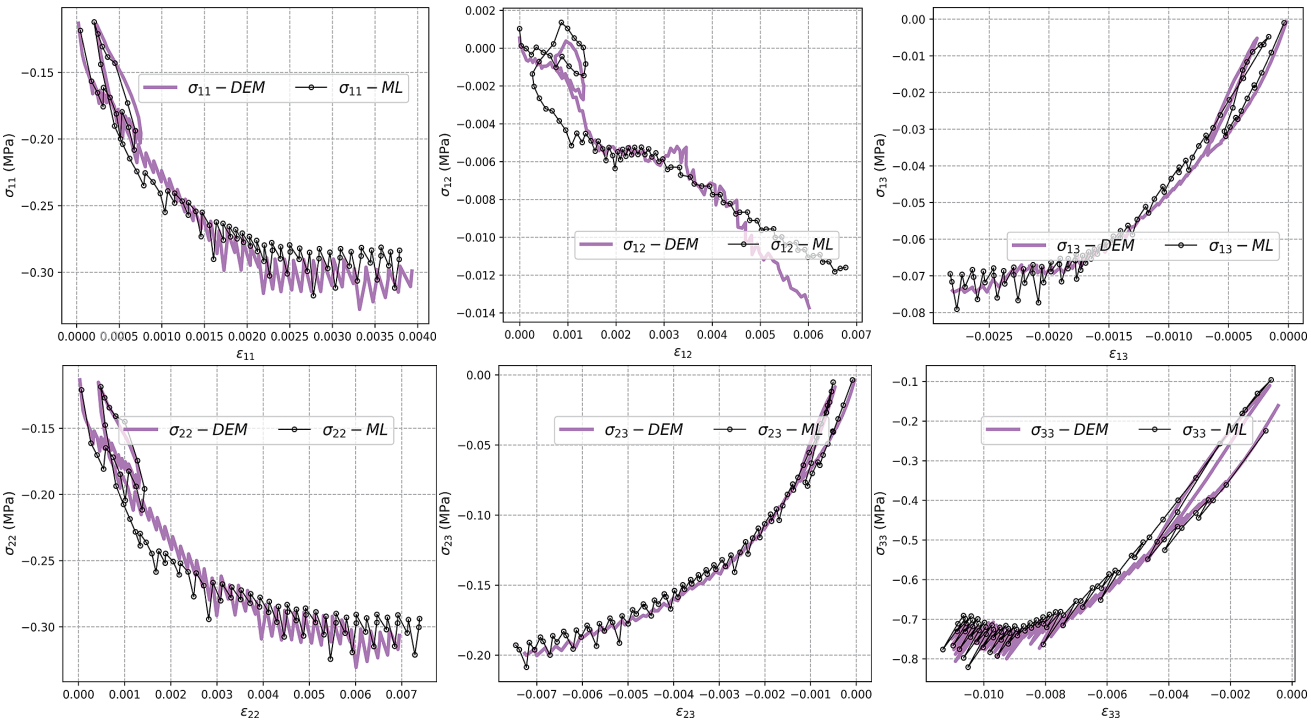

Fig. 11 The predicted stress–strain response at Gaussian point A.

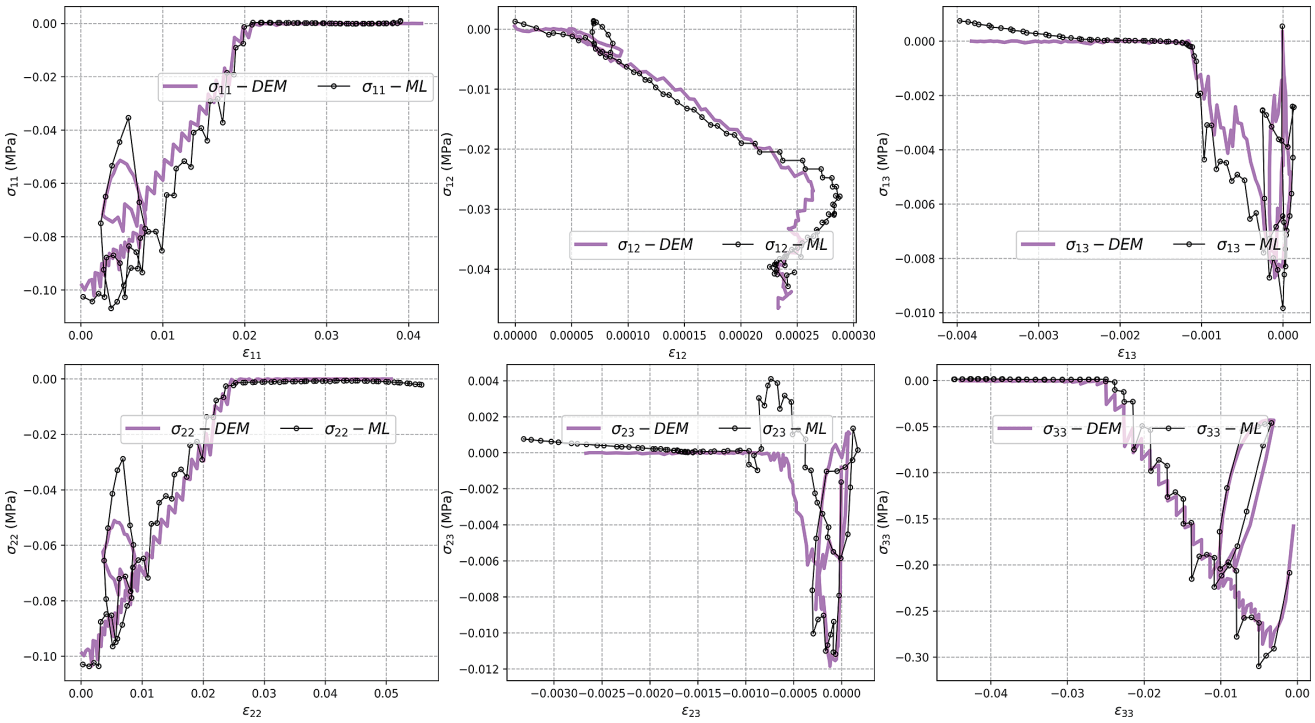

Fig. 12 The predicted stress–strain response at Gaussian point B.

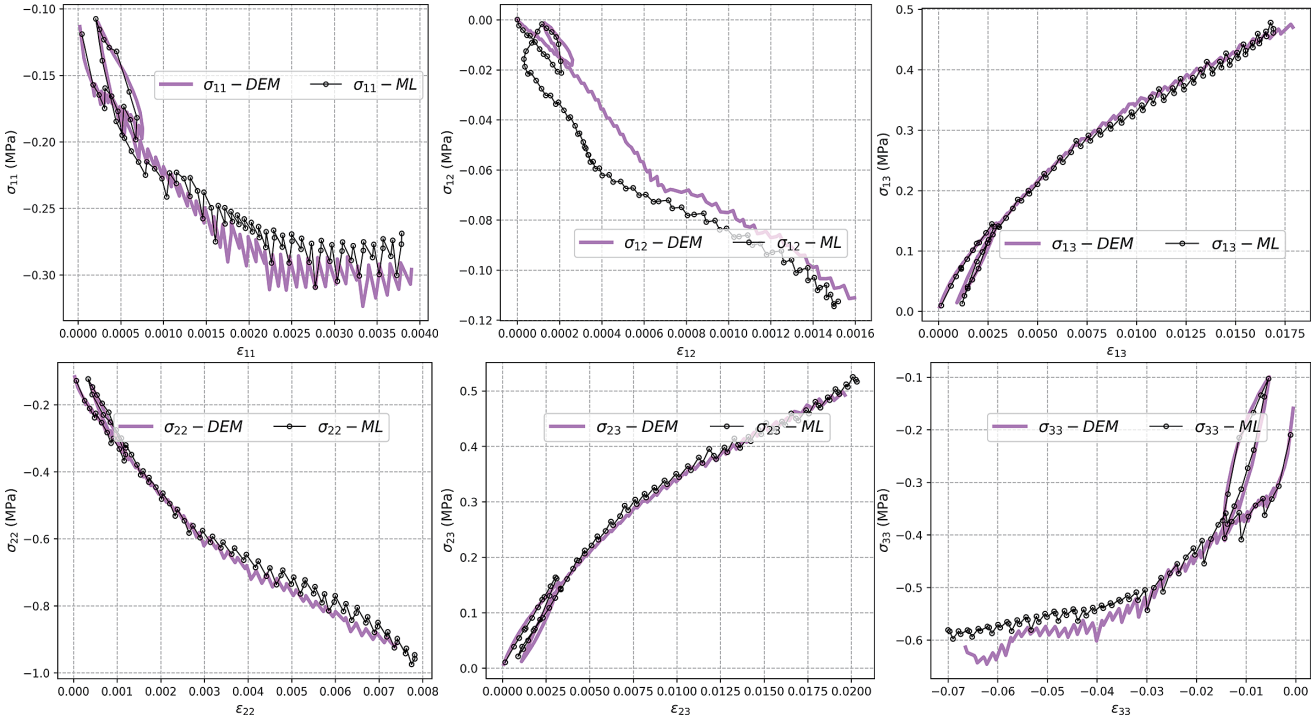

Fig. 13 The predicted stress–strain response at Gaussian point C.

Table 4 Experimental parameters of the FEM–DEM and FEM–ML triaxial compression models.

Method	Loading path	Total load steps	Time (h)	Unloading step	Reloading step	Number of RVEs
FEM–DEM	*Path2*	57	24.8	10	16	2000
FEM–ML	*Path2*	57	0.2	10	16	2000

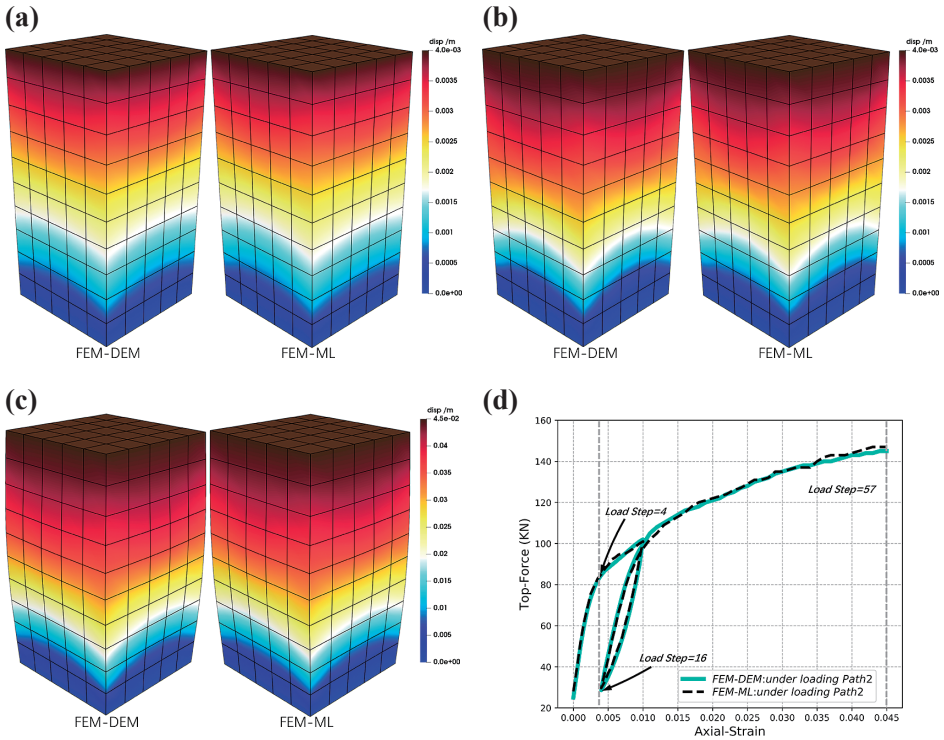

Fig. 14 Axial displacement fields solved by FEM–DEM and FEM–ML: **(a)** Load step = 4; **(b)** Load step = 16; **(c)** Load step = 57; **(d)** The top force.

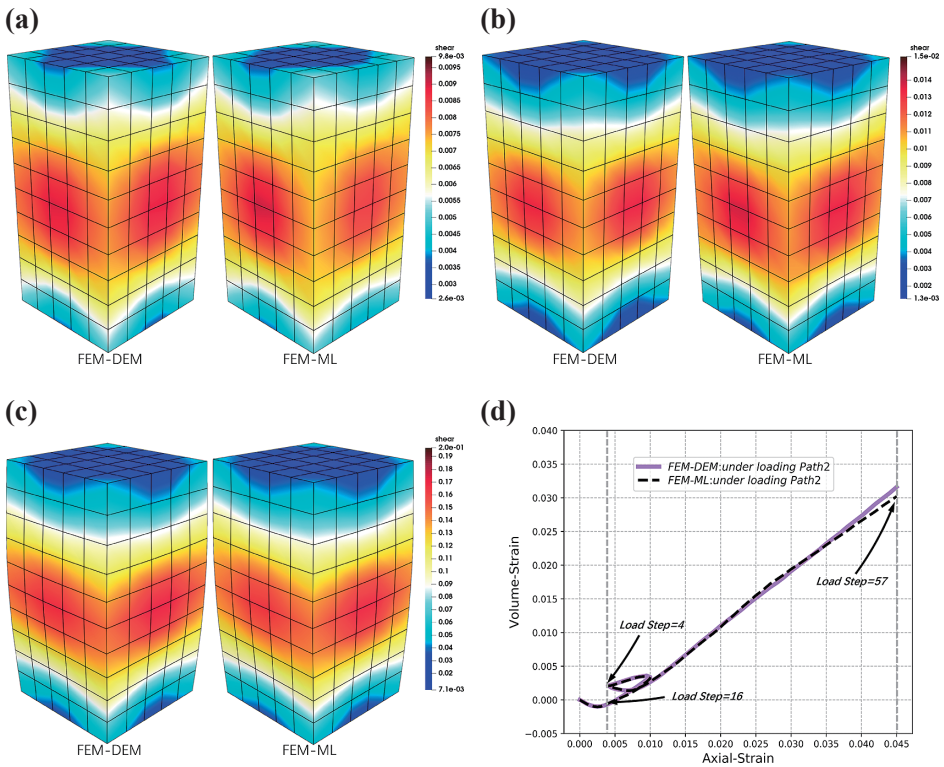

Fig. 15 Solved shear strain fields by FEM–DEM and FEM–ML: **(a)** Load step = 4; **(b)** Load step = 16; **(c)** Load step = 57; **(d)** The top force.

The simulation results obtained by both the FEM–DEM and FEM–ML approaches demonstrate that the developed FEM–ML can successfully replicate the macroscopic deformation features of granular materials under the loading *Path2*. This indicates that the trained MLPs in **Section 3.2** perform well at each Gaussian point of the FE mesh to predict the history-dependent constitutive behaviours of local materials under different loading paths, i.e. *Path2*, even though their training data comes from the FEM–DEM modelling under loading *Path1*. Furthermore, the results

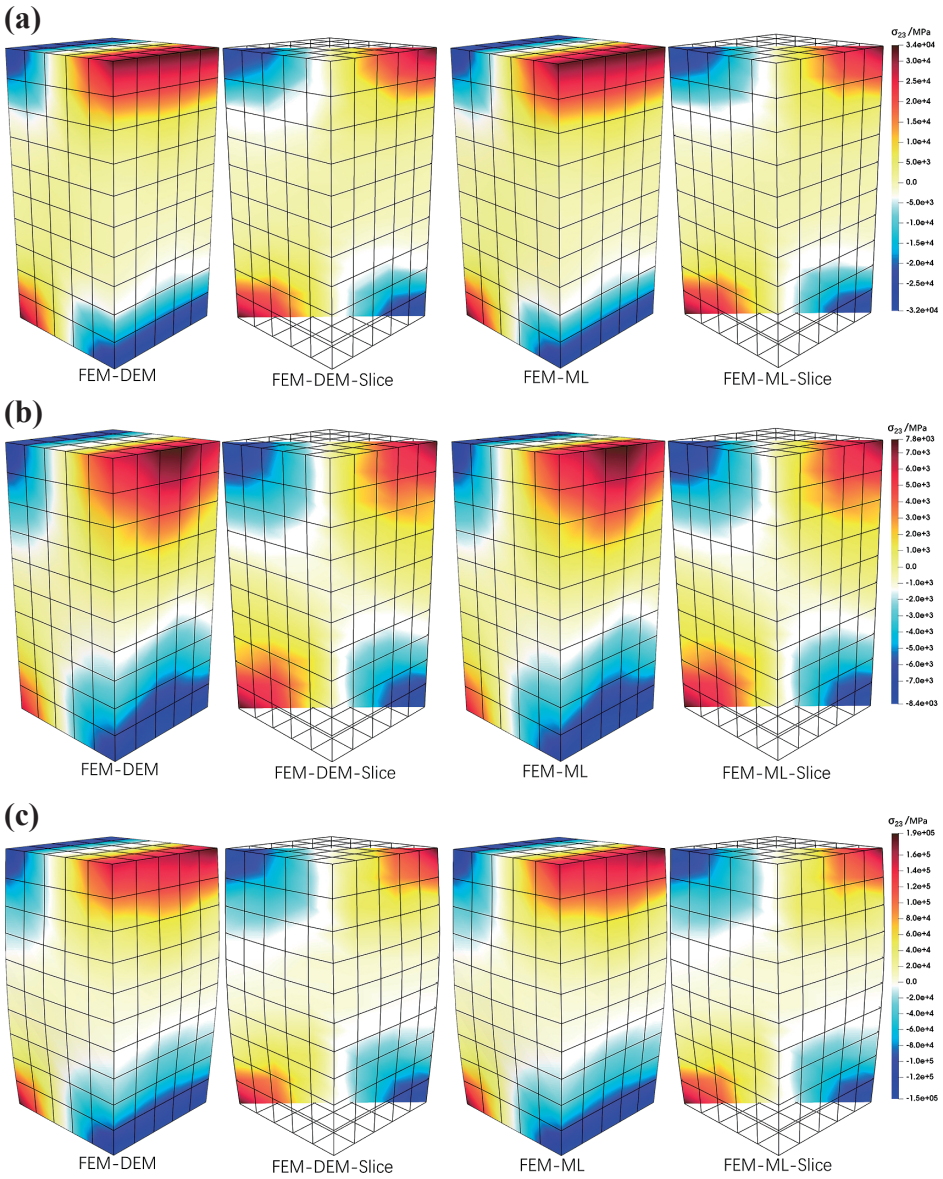

Fig. 16 Stress fields solved by FEM–DEM and FEM–ML: **(a)** Load step = 4; **(b)** Load step = 16; **(c)** Load step = 57.

displayed in **Figs. 14(d)** and **15(d)** demonstrate that the top force and volume strain of the computational domain solved by the FEM–ML method remain highly consistent with those acquired by the FEM–DEM modelling.

Additionally, as another significant metric to assess the proposed FEM–ML scheme, the stress fields of the stress components obtained by both numerical methods were compared. For instance, **Fig. 16** shows the shear stress σ_{23} at the 4th, 16th and 57th loading steps along with the corresponding slice of each modelling result. These comparison results further demonstrate that the trained NN_{σ} and NN_{D} have comparable performance to the DEM solver in providing the history-dependent constitutive response and tangent stiffness matrix for each Gaussian point in the FEM.

4. Conclusion

This study presents a novel history-information-embedded FEM–ML approach that leverages MLP models to provide the stress–strain response for each Gaussian point to significantly enhance the computational efficiency of the conventional FEM–DEM multiscale method for 3D problems. To enable the single-step-based neural network to effectively capture the history-dependent constitutive behaviours of granular media, three innovative state variable-based internal variables were integrated into the MLP model as additional input features to construct the history-information-encoded FEM–ML multiscale framework. The developed data-driven multiscale approach was comprehensively validated through the solution of the BVP of conventional triaxial compression. The results obtained by the FEM–ML method were systematically compared with those derived from the FEM–DEM method under

identical BVP and loading conditions.

The comparison reveals that the MLP model coupled with the proposed history variables for the granular material satisfactorily provides the local constitutive response of each Gaussian point, effectively substituting the DEM solver within the FEM framework. Additionally, the macroscopic modelling results using the proposed data-driven multiscale method are highly consistent with those of traditional FEM–DEM simulation. The results demonstrate that the developed FEM–ML method achieves comparable performance to the traditional FEM–DEM algorithm in triaxial compression modelling but with approximately 125 times the computational efficiency, indicating its potential as a highly efficient alternative to the conventional FEM–DEM algorithm for 3D simulations.

Nomenclature

ML	machine learning
MLP	multi-layer perceptron
RVE	representative volume element
FEM	finite element method
DEM	discrete element method
CTC	conventional triaxial compression
RNN	recurrent neural network
TCNN	temporal convolutional neural network
GRU	gated recurrent unit
LSTM	long short-term memory
AD	automatic differentiation
BVP	boundary value problem

References

Andrade J.E., Avila C.F., Hall S.A., Lenoir N., Viggiani G., Multiscale modeling and characterization of granular matter: From grain kinematics to continuum mechanics, Journal of the Mechanics and Physics of Solids, 59 (2011) 237–250. https://doi.org/10.1016/j.jmps.2010.10.009

Andrade J.E., Tu X., Multiscale framework for behavior prediction in granular media, Mechanics of Materials, 41 (2009) 652–669. https://doi.org/10.1016/j.mechmat.2008.12.005

Basheer I.A., Selection of methodology for neural network modeling of constitutive hystereses behavior of soils, Computer-Aided Civil and Infrastructure Engineering, 15 (2000) 445–463. https://doi.org/10.1111/0885-9507.00206

Basheer I.A., Stress-strain behavior of geomaterials in loading reversal simulated by time-delay neural networks, Journal of Materials in Civil Engineering, 14 (2002) 270–273. https://doi.org/10.1061/(ASCE)0899-1561(2002)14:3(270)

Desrues J., Andò E., Strain localisation in granular media, Comptes Rendus Physique, 16 (2015) 26–36. https://doi.org/10.1016/j.crhy.2015.01.001

Drakos S., Pande G., On neural network constitutive models for geomaterials, Journal of Civil Engineering Research, 5 (2015) 106–113. https://doi.org/10.5923/j.jce.20150505.02

Geers M.G.D., Kouznetsova V.G., Brekelmans W.A.M., Multi-scale computational homogenization: trends and challenges, Journal of Computational and Applied Mathematics, 234 (2010) 2175–2182. https://doi.org/10.1016/j.cam.2009.08.077

Ghavamian F., Simone A., Accelerating multiscale finite element simulations of history-dependent materials using a recurrent neural network, Computer Methods in Applied Mechanics and Engineering, 357 (2019) 112594. https://doi.org/10.1016/j.cma.2019.112594

Gross L., Bourgouin L., Hale A.J., Mühlhaus H.B., Interface modeling in incompressible media using level sets in Escript, Physics of the Earth and Planetary Interiors, 163 (2007) 23–34. https://doi.org/10.1016/j.pepi.2007.04.004

Guo N., Zhao J., A coupled FEM/DEM approach for hierarchical multiscale modelling of granular media, International Journal for Numerical Methods in Engineering, 99 (2014) 789–818. https://doi.org/10.1002/nme.4702

Guo N., Zhao J., 3D multiscale modeling of strain localization in granular media, Computers and Geotechnics, 80 (2016) 360–372. https://doi.org/10.1016/j.compgeo.2016.01.020

Hashash Y.M.A., Jung S., Ghaboussi J., Numerical implementation of a neural network based material model in finite element analysis, International Journal for Numerical Methods in Engineering, 59 (2004) 989–1005. https://doi.org/10.1002/nme.905

Hashash Y.M.A., Song H., The integration of numerical modeling and physical measurements through inverse analysis in geotechnical engineering, KSCE Journal of Civil Engineering, 12 (2008) 165–176. https://doi.org/10.1007/s12205-008-0165-2

Hu X., Zhang Y., Guo L., Wang J., Cai Y., Fu H., Cai Y., Cyclic behavior of saturated soft clay under stress path with bidirectional shear stresses, Soil Dynamics and Earthquake Engineering, 104 (2018) 319–328. https://doi.org/10.1016/j.soildyn.2017.10.016

Huang D., Fuhg J.N., Weißenfels C., Wriggers P., A machine learning based plasticity model using proper orthogonal decomposition, Computer Methods in Applied Mechanics and Engineering, 365 (2020) 113008. https://doi.org/10.1016/j.cma.2020.113008

Kruyt N.P., Rothenburg L., Statistical theories for the elastic moduli of two-dimensional assemblies of granular materials, International Journal of Engineering Science, 36 (1998) 1127–1142. https://doi.org/10.1016/S0020-7225(98)00003-2

Li X., Liu Q., Zhang J., A micro–macro homogenization approach for discrete particle assembly – Cosserat continuum modeling of granular materials, International Journal of Solids and Structures, 47 (2010) 291–303. https://doi.org/10.1016/j.ijsolstr.2009.09.033

Logarzo H.J., Capuano G., Rimoli J.J., Smart constitutive laws: inelastic homogenization through machine learning, Computer Methods in Applied Mechanics and Engineering, 373 (2021) 113482. https://doi.org/10.1016/j.cma.2020.113482

Ma G., Guan S., Wang Q., Feng Y.T., Zhou W., A predictive deep learning framework for path-dependent mechanical behavior of granular materials, Acta Geotechnica, 17 (2022) 3463–3478. https://doi.org/10.1007/s11440-021-01419-y

Miehe C., Dettmar J., Zäh D., Homogenization and two-scale simulations of granular materials for different microstructural constraints, International Journal for Numerical Methods in Engineering, 83 (2010) 1206–1236. https://doi.org/10.1002/nme.2875

Qu T., Di S., Feng Y.T., Wang M., Zhao T., Towards data-driven constitutive modelling for granular materials via micromechanics-informed deep learning, International Journal of Plasticity, 144 (2021) 103046. https://doi.org/10.1016/j.ijplas.2021.103046

Qu T., Feng Y.T., Zhao J., A strain energy-based elastic parameter calibration method for lattice/bonded particle modelling of solid materials, Powder Technology, 410 (2022) 117860. https://doi.org/10.1016/j.powtec.2022.117860

Qu T., Guan S., Feng Y.T., Ma G., Zhou W., Zhao J., Deep active learning for constitutive modelling of granular materials: from representative volume elements to implicit finite element modelling, International Journal of Plasticity, 164 (2023) 103576. https://doi.org/10.1016/j.ijplas.2023.103576

Sidarta D.E., Ghaboussi J., Constitutive modeling of geomaterials from non-uniform material tests, Computers and Geotechnics, 22 (1998) 53–71. https://doi.org/10.1016/S0266-352X(97)00035-9

Smilauer V., Angelidakis V., Catalano E., Caulk R., Chareyre B., Chevremont W., Dorofeenko S., Duriez J., Dyck N., Elias J., et al.,Yade documentation, arXiv preprint, (2023) arXiv:2301.00611. https://doi.org/10.48550/arXiv.2301.00611

Thornton C., Numerical simulations of deviatoric shear deformation of granular media, Géotechnique, 50 (2000) 43–53. https://doi.org/10.1680/geot.2000.50.1.43

Tian Y., Yao Y.-P., Modelling the non-coaxiality of soils from the view of cross-anisotropy, Computers and Geotechnics, 86 (2017) 219–229.

https://doi.org/10.1016/j.compgeo.2017.01.013
Wang M.Q., Feng Y.T., Guan S., Qu T., Multi-layer perceptron-based data-driven multiscale modelling of granular materials with a novel Frobenius norm-based internal variable, Journal of Rock Mechanics and Geotechnical Engineering, 16 (2024) 2198–2218. https://doi.org/10.1016/j.jrmge.2024.02.003
Wang M.Q., Qu T., Guan S., Zhao T., Liu B., Feng Y.T., Data-driven strain–stress modelling of granular materials via temporal convolution neural network, Computers and Geotechnics, 152 (2022) 105049. https://doi.org/10.1016/j.compgeo.2022.105049
Wang M., Zhang D.Z., Deformation accommodating periodic computational domain for a uniform velocity gradient, Computer Methods in Applied Mechanics and Engineering, 374 (2021) 113607. https://doi.org/10.1016/j.cma.2020.113607
Yin Z.-Y., Chang C.S., Karstunen M., Hicher P.-Y., An anisotropic elastic–viscoplastic model for soft clays, International Journal of Solids and Structures, 47 (2010) 665–677. https://doi.org/10.1016/j.ijsolstr.2009.11.004
Zhang P., Yang Y., Yin Z.-Y., BiLSTM-based soil–structure interface modeling, International Journal of Geomechanics, 21 (2021) 04021096. https://doi.org/10.1061/(ASCE)GM.1943-5622.0002058

Authors' Short Biographies

Dr. Mengqi Wang was awarded his doctoral degree in 2025 at the Zienkiewicz Centre for Computational Engineering, Swansea University, UK. His research interests include (1) machine learning-based constitutive model; (2) multi-scale FEM-DEM method for granular materials; (3) data-driven-based FEM-ML multiscale method; and (4) continuum-based particle methods, such as MPM and SPH. His works have been presented at European academic conferences, such as the 9th Discrete Element Method (DEM9), the 21st UK Travelling Workshop–Geomechanics: From Micro to Macro, and the UK Association for Computational Mechanics (UKACM).

Dr. Min Wang is a Staff Scientist in the Fluid Dynamics and Solid Mechanics Group at the Theoretical Division of Los Alamos National Laboratory (LANL), USA. He received his Ph.D. in computational mechanics from Swansea University in 2016, specializing in DEM-LBM/CFD. He previously worked at Rockfield Software Ltd. as a project engineer, developing FEM for geomechanics applications. Since joining LANL in 2018, he has conducted research on multiscale modeling of material deformation and multiphase flow using high-resolution CFD-DEM simulations. His interests span geomechanics, solid/fluid mechanics, and machine learning applications. He has published over 50 papers and serves on editorial boards of several international journals.

Dr. Shaoheng Guan obtained his PhD degree at Wuhan University in 2023. He has been a joint Ph.D. student at Swansea University for two years during his doctoral study. Then, he joined the Graz University of Technology as a postdoctoral research assistant. His research interests include (1) phenomenological model for granular media; (2) explicit FEM modelling method for granular materials; (3) data-driven-based FEM-ML multiscale method; and (4) the large-scale deformation of nonlinear elastic material. His works have been presented at European academic conferences, such as the UK Association for Computational Mechanics (UKACM).

Prof. Yuntian Feng is a faculty member at the Zienkiewicz Centre for Computational Engineering, Swansea University, UK. He has extensive expertise in DEM and multiscale computational methods. His research mainly focuses on advancing DEM, particularly in contact detection and resolution for non-spherical particles, as well as its coupling with continuum methods such as FEM and CFD. Additionally, he specializes in large-scale high-performance computing for granular materials. Prof. Feng has authored over 150 journal articles, serves on the editorial boards of leading scientific journals, and has led multiple research projects funded by UKRI, the EU, and industry collaborators.